GEOPHYSICAL RESEARCH LETTERS, VOL. 37, L13303, doi:10.1029/2010GL043158, 2010

Present-day principal horizontal stress orientations in the Kumano forearc basin of the southwest Japan subduction zone determined from IODP NanTroSEIZE drilling Site C0009

Weiren Lin,[1] Mai-Linh Doan,[2] J. Casey Moore,[3] Lisa McNeill,[4] Timothy B. Byrne,[5] Takatoshi Ito,[6] Demian Saffer,[7] Marianne Conin,[8] Masataka Kinoshita,[9] Yoshinori Sanada,[10] Kyaw Thu Moe,[10] Eiichiro Araki,[9] Harold Tobin,[11] David Boutt,[12] Yasuyuki Kano,[13] Nicholas W. Hayman,[14] Peter Flemings,[14] Gary J. Huftile,[15] Deniz Cukur,[16] Christophe Buret,[17] Anja M. Schleicher,[18] Natalia Efimenko,[19] Kuniyo Kawabata,[20] David M. Buchs,[21] Shijun Jiang,[22] Koji Kameo,[23] Keika Horiguchi,[24] Thomas Wiersberg,[25] Achim Kopf,[26] Kazuya Kitada,[9] Nobuhisa Eguchi,[10] Sean Toczko,[10] Kyoma Takahashi,[10] and Yukari Kido[10]

Received 6 March 2010; revised 7 May 2010; accepted 12 May 2010; published 2 July 2010.

[1] A 1.6 km riser borehole was drilled at site C0009 of the NanTroSEIZE, in the center of the Kumano forearc basin, as a landward extension of previous drilling in the southwest Japan Nankai subduction zone. We determined principal horizontal stress orientations from analyses of borehole breakouts and drilling-induced tensile fractures by using wireline logging formation microresistivity images and caliper data. The maximum horizontal stress orientation at C0009 is approximately parallel to the convergence vector between the Philippine Sea plate and Japan, showing a slight difference with the stress orientation which is perpendicular to the plate boundary at previous NanTroSEIZE sites C0001, C0004 and C0006 but orthogonal to the stress orientation at site C0002, which is also in the Kumano forearc basin. These data show that horizontal stress orientations are not uniform in the forearc basin within the surveyed depth range and suggest that oblique plate motion is being partitioned into strike-slip and thrusting. In addition, the stress orientations at site C0009 rotate clockwise from basin sediments into the underlying accretionary prism.
Citation: Lin, W., et al. (2010), Present-day principal horizontal stress orientations in the Kumano forearc basin of the southwest Japan subduction zone determined from IODP NanTroSEIZE drilling Site C0009, *Geophys. Res. Lett.*, *37*, L13303, doi:10.1029/2010GL043158.

1. Introduction

[2] The Nankai Trough Seismogenic Zone Experiment (NanTroSEIZE), a comprehensive scientific drilling project conducted by the Integrated Ocean Drilling Program (IODP), began in 2007 in the Nankai subduction zone, southwest Japan, where M8-class great earthquakes repeat at intervals of 100–200 years as a result of the convergence of the Philippine Sea and Eurasian plates. Establishing the in situ stress state along active subduction zones is critical for understanding the accumulation and release of most of Earth's seismic energy [*Lallemand and Funiciello*, 2009]. Determi-

[1]Kochi Institute for Core Sample Research, JAMSTEC, Nankoku, Japan.
[2]Laboratoire de Géophysique et Tectonophysique, Université Grenoble 1 (Joseph Fourier), Grenoble, France.
[3]Earth and Planetary Sciences Department, University of California, Santa Cruz, California, USA.
[4]National Oceanography Centre, Southampton, University of Southampton, Southampton, UK.
[5]Center for Integrative Geosciences, University of Connecticut, Storrs, Connecticut, USA.
[6]Institute of Fluid Science, Tohoku University, Sendai, Japan.
[7]Geosciences, Pennsylvania State University, University Park, Pennsylvania, USA.
[8]CEREGE, University Aix Marseille III, Aix-en-Provence, France.
[9]Institute for Research on Earth Evolution, JAMSTEC, Yokosuka, Japan.
[10]Center for Deep Earth Exploration, JAMSTEC, Yokohama, Japan.
[11]Department of Geoscience, University of Wisconsin-Madison, Madison, Wisconsin, USA.
[12]Department of Geosciences, University of Massachusetts Amherst, Amherst, Massachusetts, USA.
[13]Research Center for Earthquake Prediction, Disaster Prevention Research Institute, Kyoto University, Uji, Japan.
[14]Institute for Geophysics, Jackson School of Geosciences, University of Texas at Austin, Austin, Texas, USA.
[15]Biogeosciences Discipline, Queensland University of Technology, Brisbane, Queensland, Australia.
[16]Leibniz Institute of Marine Sciences at Kiel University (IFM-GEOMAR), Kiel, Germany.
[17]Département de Géologie, Université de Picardie Jules Verne, Amiens, France.
[18]Department of Geological Sciences, University of Michigan, Ann Arbor, Michigan, USA.
[19]Institut de Géologie et de Paléontologie, Université de Lausanne, Lausanne-Dorigny, Switzerland.
[20]Institute of Geophysics, National Central University, Taoyuan, Taiwan.
[21]Research School of Earth Sciences, The Australian National University, Canberra, ACT, Australia.
[22]Geological Sciences, Florida State University, Tallahassee, Florida, USA.
[23]Department of Earth Sciences, Chiba University, Chiba, Japan.
[24]Department of Earth and Space Sciences, Osaka University, Toyonaka, Japan.
[25]Section 4.2, GFZ German Research Center for Geosciences, Potsdam, Germany.
[26]Marum Research Centre, University of Bremen, Bremen, Germany.

0094-8276/10/2010GL043158

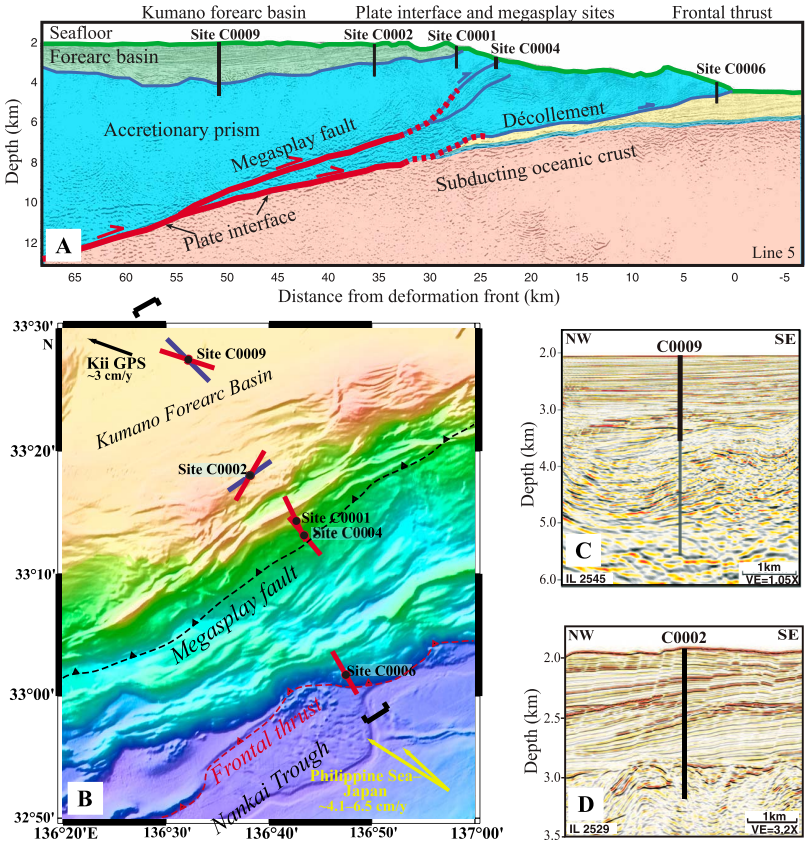

Figure 1. Location and setting of NanTroSEIZE site C0009. (a) Locations of NanTroSEIZE drilling sites and structure of the Nankai subduction zone. Seismic reflection section is after *Park et al.* [2002]. (b) Bathymetric map of the drilling sites and their maximum principal horizontal stress (S_{Hmax}) orientations. Bars at the drilling sites show the S_{Hmax} orientations in boreholes. Blue bars show stress orientations in the accretionary prism below 1285 mbsf at C0009 and below 936 mbsf at C0002 [*Tobin et al.*, 2009]. Dashed lines show megasplay fault and frontal thrust [*Moore et al.*, 2007]. Brackets show location of the cross-section in Figure 1a. Yellow arrows show the far-field convergence vectors between the Philippine Sea plate and Japan [*Heki and Miyazaki*, 2001]; black arrow shows far-field plate motion vector based on geodetic results [*Heki and Miyazaki*, 2001]. (c) Seismic reflection profile through site C0009. The wider line shows interval drilled in 2009, and the narrow line shows planned future drilling. (d) Seismic reflection profile through site C0002. The seismic profiles of Figures 1c and 1d are after *Araki et al.* [2009].

nation of in situ stress is one of the most important scientific objectives of NanTroSEIZE, and also one of the major goals of the IODP as the seismogenic parts of plate margins are often only accessible through drilling.

[3] More than 10 vertical boreholes have been drilled to date along the NanTroSEIZE transect, which is approximately orthogonal to the Nankai Trough axis (plate boundary). In the first stage of NanTroSEIZE (2007–2008), stress orientations were determined from drilling-induced compressive failures (breakouts) and drilling-induced tensile fractures (DITFs) observed in borehole wall images obtained by logging while drilling (LWD) technology [e.g., *Tobin et al.*, 2009; *Chang et al.*, 2009]. This stage involved four drilling sites in which LWD was performed: the initial faulting (frontal thrust) site C0006 at the toe of the accretionary prism, the megasplay sites C0004 and C0001, and site C0002 in the southeastern part of the Kumano forearc basin (Figure 1). In addition, *Byrne et al.* [2009] applied the anelastic strain recovery (ASR) technique to drill-core samples to constrain three-dimensional stress orientations. These consistent results showed that the maximum principal horizontal stress (S_{Hmax}) orientations at sites C0006, C0004, and C0001 are generally orthogonal to the plate boundary. However, at site C0002, located at the shelf break, these same methods showed that the S_{Hmax} orientation is approximately parallel to the plate boundary. This result is also consistent with seismic reflection profiles and core-scale fault data [*Byrne et al.*, 2009]. Thus, it is of great interest to know the stress orientation farther landward along the NanTroSEIZE transect (northwest of site C0002) in the basin.

[4] During IODP Expedition 319 in the second stage of NanTroSEIZE, D/V *Chikyu* carried out borehole drilling at site C0009, above the asperity of the 1944 Tonankai M8.1 earthquake in the Nankai subduction zone. The borehole penetrated the Kumano basin sediments and the underlying accretionary prism. In a depth range from approximately 700 mbsf (meters below seafloor) to the target depth of 1600 mbsf, wireline logging was carried out including caliper, the Fullbore Formation MicroImager (FMI) borehole resistivity images and porosity, P and S wave velocities, resistivity [*Saffer et al.*, 2009]. We used the borehole images and caliper data to identify DITFs and breakouts that could be interpreted in terms of principal horizontal stress

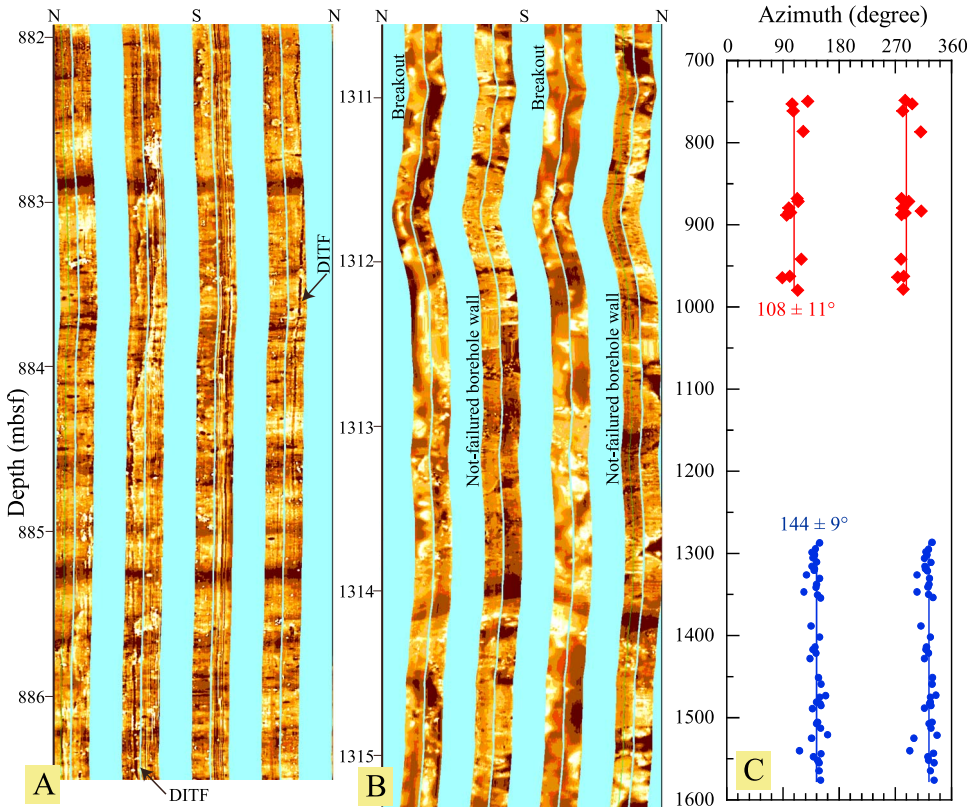

Figure 2. Borehole wall images and S_{Hmax} orientaions at site C0009. (a) Electrical images of borehole walls around 884 mbsf showing drilling-induced tensile fractures (DITFs). Blank regions between columns are unimaged portions of the borehole wall between the FMI arms. (b) Electrical image around 1313 mbsf showing breakouts. (c) S_{Hmax} azimuthal distribution determined from DITFs (diamonds) and breakouts (circles). Vertical lines show the average azimuths, and numbers show the average azimuth values and their standard deviations.

orientations [*Zoback et al.*, 2003; *McNeill et al.*, 2004; *Lin et al.*, 2007].

2. Wireline Logging

[5] A deep borehole was drilled at site C0009 from the seafloor, at 2054 m water depth, to approximately 700 mbsf by traditional riserless drilling and from 700 mbsf to the target depth of 1600 mbsf by riser drilling, which was the first successful application of this technique in scientific ocean drilling. From 0 mbsf to 1285 mbsf the borehole crossed the basin and possible slope deposits of the early prism (lithologic units I–III), and from 1285 mbsf to total depth at 1600 mbsf (Unit IV) within underlying early accretionary prism sediments or slope deposits [*Saffer et al.*, 2009].

[6] Immediately after drilling reached the target depth, two runs of wireline logging were conducted from approximately 700 mbsf to 1600 mbsf. The first run included a two-arm caliper and a six-arm caliper, however, without azimuth data for the caliper arms. The second wireline logging run had azimuth information and included FMI. The FMI tool has four arms at 90° angles; an arm with a pad and a flap takes one column of FMI image (Figures 2a and 2b). Because the 12.25-inch (approximately 31 cm) drilling bit was large in comparison to the available pad-flap size, the FMI images covered only about 50% of the borehole walls (Figures 2a and 2b). The two pairs of FMI arms at the same azimuthal position with the pads also measured the borehole diameter in two orthogonal directions, serving as a four-arm caliper tool.

[7] Because both breakouts and DITFs are dependent on in situ stress conditions, we can use information on their azimuth to determine orientations of in situ principal stresses in the plane perpendicular to the borehole axis. As breakouts and DITFs are both formed during or shortly after drilling, they are records of the present-day stress state. The borehole FMI images enable both the breakouts and DITFs to be identified and the horizontal stress orientations to be determined. In principle, the width (span) of breakouts can constrain the S_{Hmax} magnitude on the basis of the minimum principal horizontal stress (S_{hmin}) magnitude and rock compressive strength. This was difficult in practice at site C0009 because breakout width data were poorly resolved owing to the relatively poor coverage of FMI images. Usually, one pair of caliper arms stops at breakouts (elongations) because their spring forces them open wider into the breakout, therefore it is possible to determine the azimuths of breakouts from caliper data, but this is not possible for DITF data because the tensile fractures are narrower than the caliper arms. At site C0009, FMI images are a crucial supplement to caliper data, providing direct and visual evidence to characterize breakouts.

3. FMI Image Analyses for DITFs and Breakouts

[8] Over approximately 900 m of the C0009 borehole, several DITFs and many breakouts were recognized in the

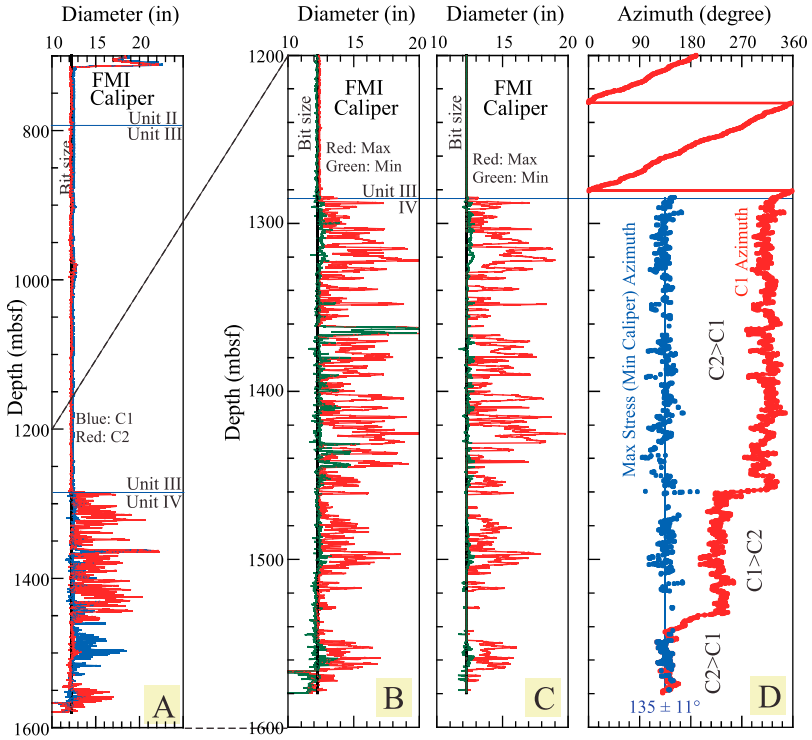

Figure 3. Caliper records from site C0009. (a) Borehole diameters determined by FMI calipers for the whole surveyed depth range. FMI calipers measure two diameters in orthogonal directions, labeled C1 and C2, every 6 inches (approximately 15 cm). Profiles in Figures 3b through 3d correspond to this profile from 1200 to 1600 mbsf. (b) Raw FMI caliper data in terms of maximum and minimum diameters. (c) Selected FMI caliper data meeting the three quality criteria given in the text. (d) C1 azimuth (red dots and line) of FMI caliper and S_{Hmax} azimuth (blue dots) determined from the selected data shown in Figure 3c. The average value and standard deviation of the S_{Hmax} azimuth is N135°E ± 11°.

FMI images (Figures 2a and 2b). The DITFs occurred in a depth range of 749–980 mbsf (forearc basin sediments and slope deposits of Pleistocene and Pliocene age, Unit II–III [*Saffer et al.*, 2009]), and the breakouts occurred in the depth range of 1288–1578 mbsf (possible accretionary prism or slope deposits, late Miocene, Unit IV). The boundary between Unit III and IV was defined by an unconformity (UC3), at 1285 mbsf, where an age gap of approximately 1.8 Ma was recognized [*Saffer et al.*, 2009]. Between 980 and 1285 mbsf (early forearc basin sediments or slope deposits, Pliocene, Unit III), neither DITF nor breakouts were found (Figure 2c). Breakouts or DITFs, if present, should be found in pairs on opposite sides of the borehole wall (180° apart), if the rock strength around the borehole are almost uniform (homogeneous lithology). DITFs should also be perpendicular to the borehole wall, hence very straight. These characteristics were valuable in distinguishing breakouts and DITFs from other borehole wall failures such as washouts and pre-existing structural fractures. Furthermore, we distinguished breakouts as being wider than fractures and without the sharp, straight boundaries of tensile fractures. Using these criteria, we recorded the azimuth data of breakouts and DITFs from the FMI images and plotted the S_{Hmax} azimuth (Figure 2c). Our analysis of DITFs and breakouts in the FMI images yielded average S_{Hmax} azimuths and its standard deviation of approximately N108°E ± 11° in the shallower depth range (749–980 mbsf, determined from 14 DITFs) and N144°E ± 9° in the deeper range (1288–1578 mbsf, 42 breakouts) (Figure 2c). The variation in the measured azimuth data probably reflects localized stress orientation changes around minor faults, fractures, and lithologic boundaries [*Lin et al.*, 2010].

[9] Because P-wave velocity increased and resistivity decreased with lithologic unit changes from III to IV [*Saffer et al.*, 2009], it is reasonable to infer the compressive strength and Young's modulus in Unit IV are higher than those in Unit III, respectively. Thus, the presence of breakouts in the stronger formation (Unit IV), and not in the weaker formation (Unit III), is interesting, because in general breakouts occur easily in weaker rock if the stress magnitudes are the same. Certainly, this observation means that stress state in Unit IV distinctly differs with that in Unit III. In principle, breakout occurs once the circumferential stress σ_c at the borehole wall in the minimum stress azimuth exceeds the rock compressive strength. This stress σ_c is expressed as $\sigma_c = 3S_{Hmax} - S_{hmin} - P_p - P_m$, where P_p and P_m are pore pressure and mud pressure, respectively [*Zoback et al.*, 2003]. Thus, σ_c is mainly controlled by S_{Hmax}. Therefore, a further possible interpretation is that the S_{Hmax} magnitude in Unit IV is higher than that in Unit III. If this interpretation is true, this suggests that the harder/stronger formation bears a higher loading than the softer/weaker formation. That is, the S_{Hmax} magnitude in accretionary prism (Unit IV) may be obviously higher than that in the forearc basin sediments (Unit III). At the same time, these observations indicate that the S_{Hmax} magnitude profile may be not a simple direct proportion relation with depth. If the

coupling strength of the unconformities is weak, it may be the other possible reason for this phenomenon except the different formation hardness.

4. Caliper Data Analyses for Breakouts

[10] The FMI caliper data showed that at depths above 1285 mbsf (in units II and III) the two orthogonal diameter profiles (C1 and C2) were almost identical, showing no clear borehole elongations, which suggests that almost no breakout occurred (Figure 3a). Clear borehole elongations were recognized, showing the presence of breakouts, below 1285 mbsf in Unit IV. All three types of caliper (two-, four- and six-arm calipers) yielded nearly the same borehole maximum diameter profiles. This reproducibility suggests that one pair of the FMI caliper arms always finds the maximum elongated position. Moreover, the azimuth of the FMI arms rotated freely in the circular part of the borehole above 1285 mbsf but indicates a dominant azimuth in the elongated part of the borehole below 1285 mbsf, even though the two caliper pairs exchanged positions at depths around 1460 and 1535 mbsf (Figure 3d). This behavior also shows that caliper arms reliably report the elongated borehole position.

[11] In identifying breakouts from the four-arm caliper data, we used three criteria for controlling data quality similar to *Plumb et al.* [1985]. First, the larger caliper diameter should be sufficiently greater than the smaller diameter such that the difference between the two diameters C1 and C2 is at least 0.05 times the drilling diameter D, in this case approximately 15 mm or 0.6 inches. Second, the smaller caliper diameter should not exceed 1.05 D. Third, both diameters should not be significantly less than the bit diameter, that is, C1 and C2 > 0.95 D. This generated a subset of the data of 1061 measurements (Figure 3c) which displays gaps due to borehole caving around 1360 mbsf and due to constriction (probably from drilling generated cuttings and/or cavings) around 1570 mbsf (compare Figures 3b and 3c). Another gap at 1520–1540 mbsf reflects a nearly circular borehole and the absence of continuous breakouts (Figure 3c).

[12] We determined the profile of S_{Hmax} azimuths below 1285 mbsf by adding 90° to the S_{hmin} azimuth shown by the orientation of maximum borehole elongation in the selected FMI caliper data (Figure 3d). The average azimuth and its standard deviation were N135°E and 11°, respectively, and showed no clear trend with depth. The average azimuth obtained from the FMI images differed by 9° from that from the caliper data, probably because poor image coverage (about 50%) resulted in inaccuracies in picking breakouts. Therefore, we believe that the stress azimuth data from caliper should be more accurate than those from FMI image.

[13] With respect to comparison of the stress orientations in shallower (obtained from DITFs (Figure 2c)) and in deeper (from caliper breakouts (Figure 3d)) ranges, there was a notable difference in azimuths from the shallower to the deeper levels; a clockwise rotation of approximately 30°. This rotation is significant because the standard deviations of the azimuth are around 10°. Similarly, at drilling site C0002 about 20 km away from C0009 in the seaward part of the Kumano forearc basin, stress orientations rotated clockwise (Figure 1b) at depths below 936 mbsf, at the transition from basin-slope deposits to prism [*Tobin et al.*, 2009].

5. Stress Orientations at NanTroSEIZE Sites

[14] In order to interpret the regional significance of the stress orientations, we need first consider the significance of the change in stress orientations with depth. The orientations at both C0009 and C0002 rotate clockwise from basin sediments to the underlying accretionary prism or prism slope deposits (Figure 1b). The stress rotation with depth might be caused by i) the effect of a strike slip fault with depth-dependent strength [e.g. *Chéry et al.*, 2004], ii) a decoupling between the basin and the accretionary wedge, and iii) reorientation of stress field across an angular unconformity that separates rocks with different elastic properties. The recent identification of strike-slip faulting along the shelf edge [*Martin et al.*, 2010] and within a few hundred meters of C0002 suggests the first cause may apply at this site. At site C0009, which is several kilometers from the fault zone at the shelf edge either cause ii or iii might apply.

[15] In the relatively shallow drilled depth range of the NanTroSEIZE sites (less than approximately 1600 mbsf at all the sites), the S_{Hmax} orientations at site C0009 was slightly different with the S_{Hmax} orientations at sites C0001, C0004, and C0006, and significantly different with the orientation at site C0002 which is closer to C0009 than the other sites (Figure 1b). In addition, the S_{Hmax} orientations at site C0009 are correlated to the plate motion. In details, the orientation at deeper depths (Unit IV) is nearly parallel to the convergence vector between the Philippine Sea plate and Japan (yellow arrows in Figure 1b); whereas the orientation at shallower depths appears to be more nearly parallel to the geodetically-determined motion of the Kii Peninsula (black arrow in Figure 1b). This parallelism between the shortening direction of Kii Peninsula and the stress orientations above the unconformity suggest that these data are more appropriate for explaining the surficial plate motion in hanging wall than the data below the unconformity. However, the S_{Hmax} orientations at sites C0001, C0004 and C0006 are more orthogonal to the margin strike. These results may imply a possible interpretation of deformation partitioning structure, that is, the oblique plate convergence is being partitioned into trench-parallel and right-lateral slip and thrusting. Evidence for right-lateral slip on east-northeast trending faults, consistent with strain partitioning, has been found along the outer-arc high in the Tokai [*Huchon et al.*, 1998] and in the To-Nankai areas [*Martin et al.*, 2010] (Figure 1b).

[16] The S_{Hmax} orientations at C0009 and C0002 are nearly at right angles to each other. A seismic reflection profile at C0002 in the basin running NW–SE (Figure 1d) displays a clear sequence of normal faults [e.g., *Tobin et al.*, 2009]. Moreover, ASR data on cores from site C0002 showed a normal fault stress regime, indicating an extensional deformation pattern [*Byrne et al.*, 2009]. These results are consistent with the stress orientation at C0002 being perpendicular to the plate boundary. In contrast to C0002, normal faulting is more sparse in the landward part of the basin, in the vicinity of cite C0009 (Figure 1c).

6. Conclusions

[17] In the borehole at NanTroSEIZE site C0009, we determined horizontal stress orientations at the center of the Kumano forearc basin in the Nankai subduction zone, Japan. We identified and characterized borehole breakouts and drilling-induced tensile fractures by using wireline logging FMI images and caliper data.

[18] Among the four NanTroSEIZE sites drilled before C0009, three (C0001, C0004, and C0006) show S_{Hmax} almost orthogonal to the plate boundary, whereas the forth site, C0002, drilled at the seaward edge of the basin, shows S_{Hmax} parallel to the shelf edge or plate boundary. In contrast to these results, new stress orientation results obtained in this study at site C0009 at the center of the Kumano forearc basin show S_{Hmax} generally parallel to the convergence direction. Overall, the regional stress patterns suggest strain partitioning during oblique plate convergence. The boreholes penetrated through basin sediments into the underlying accretionary prism and/or slope deposits at both sites C0009 and C0002, and at both sites the stress orientations rotated clockwise, indicating changes of stress state with depth. In addition, the presence of breakouts in Unit IV, and not in Unit III at C0009, possibly suggests that S_{Hmax} magnitude in accretionary prism (Unit IV) may be higher than that in the forearc basin sediments or slope deposits (Unit III).

[19] **Acknowledgments.** This research used data provided by the IODP. The authors gratefully acknowledge the support provided by the D/V *Chikyu* drilling crew, logging staff, and laboratory technicians. Discussions with Asuka Yamaguchi and Pierre Henry were helpful for preparing the manuscript. Part of this work was supported by Grants-in-Aid for Scientific Research 19540453, 22403008 (JSPS), and 21107006 (MEXT), Japan.

References

Araki, E., T. Byrne, L. McNeill, D. Saffer, N. Eguchi, K. Takahashi, and S. Toczko (2009), NanTroSEIZE Stage 2: NanTroSEIZE riser/riserless observatory, *Integr. Ocean Drill. Program Sci. Prosp.*, *319*, doi:10.2204/iodp.sp.319.2009.

Byrne, T. B., et al. (2009), Anelastic strain recovery reveals extension across SW Japan subduction zone, *Geophys. Res. Lett.*, *36*, L23310, doi:10.1029/2009GL040749.

Chang, C., et al. (2009), Constraining in situ stress tensor in the Kumano forearc basin, Nankai, based on borehole wall failure analysis, *Eos Trans. AGU*, *90*(52), Fall Meet. Suppl., Abstract T21C-1832.

Chéry, J., M. D. Zoback, and S. Hickman (2004), A mechanical model of the San Andreas fault and SAFOD Pilot Hole stress measurements, *Geophys. Res. Lett.*, *31*, L15S13, doi:10.1029/2004GL019521.

Heki, K., and S. Miyazaki (2001), Plate convergence and long-term crustal deformation in central Japan, *Geophys. Res. Lett.*, *28*, 2313–2316, doi:10.1029/2000GL012537.

Huchon, P., et al. (1998), Pervasive dextral strike-slip faulting within the backstop of the Eastern Nankai wedge confirmed by the deep-towed seismic data (Kaiko-Tokai 1996 cruise), *C. R. Acad. Sci.*, *326*, 869–875.

Lallemand, S., and F. Funiciello (2009), *Subduction Zone Geodynamics*, doi:10.1007/978-3-540-87974-9, Springer, Berlin.

Lin, W., et al. (2007), Current stress state and principal stress rotations in the vicinity of the Chelungpu fault induced by the 1999 Chi-Chi, Taiwan, earthquake, *Geophys. Res. Lett.*, *34*, L16307, doi:10.1029/2007GL030515.

Lin, W., et al. (2010), Localized rotation of principal stress around faults and fractures determined from borehole breakouts in hole B of the Taiwan Chelungpu-fault Drilling Project (TCDP), *Tectonophysics*, *482*, 82–91, doi:10.1016/j.tecto.2009.06.020.

Martin, K. M., et al. (2010), Possible strain partitioning structure between the Kumano forearc basin and the slope of the Nankai Trough accretionary prism, *Geochem. Geophys. Geosyst.*, *11*, Q0AD02, doi:10.1029/2009GC002668.

McNeill, L. C., M. Ienaga, H. Tobin, S. Saito, D. Goldberg, J. C. Moore, and H. Mikada, (2004), Deformation and in situ stress in the Nankai Accretionary Prism from resistivity-at-bit images, ODP Leg 196, *Geophys. Res. Lett.*, *31*, L02602, doi:10.1029/2003GL018799.

Moore, G., et al. (2007), Three-dimensional splay fault geometry and implications for tsunami generation, *Science*, *318*, 1128–1131, doi:10.1126/science.1147195.

Park, J.-O., et al. (2002), Splay fault branching along the Nankai subduction zone, *Science*, *297*, 1157–1160, doi:10.1126/science.1074111.

Plumb, R. A., et al. (1985), Stress induced borehole elongation: comparison 769 between the four-arm dip meter and the borehole televiewer in the Auburn 770 geothermal well, *J. Geophys. Res.*, *90*, 5513–5521, doi:10.1029/JB090iB07p05513.

Saffer, D., et al. (2009), NanTroSEIZE Stage 2: NanTroSEIZE riser/riserless observatory, *Integr. Ocean Drill. Program Prelim. Rep.*, *319*, doi:10.2204/iodp.pr.319.2009.

Tobin, H., et al. (2009), Expedition 314 summary, in *NanTroSEIZE Stage 1: Investigations of Seismogenesis, Nankai Trough, Japan*, *Proc. Integr. Ocean Drill. Program*, *314/315/316*, doi:10.2204/iodp.proc.314315316.111.2009.

Zoback, M. D., et al. (2003), Determination of stress orientation and magnitude in deep wells, *Int. J. Rock Mech. Min. Sci.*, *40*, 1049–1076.

E. Araki, M. Kinoshita, and K. Kitada, Institute for Research on Earth Evolution, JAMSTEC, Natsushima-cho 2-15, Yokosuka 237-0061, Japan.

D. Boutt, Department of Geosciences, University of Massachusetts Amherst, 611 North Pleasant St., Amherst, MA 01003, USA.

D. M. Buchs, Research School of Earth Sciences, The Australian National University, 61 Mills Rd., Bldg. J1, Canberra, ACT 0200, Australia.

C. Buret, Département de Géologie, Université de Picardie Jules Verne, 33, rue Saint Leu, F-80039 Amiens CEDEX, France.

T. B. Byrne, Center for Integrative Geosciences, University of Connecticut, 354 Mansfield Rd., Storrs, CT 06269, USA.

M. Conin, CEREGE, University Aix Marseille III, F-13545 Aix-en-Provence CEDEX, France.

D. Cukur, Leibniz Institute of Marine Sciences at Kiel University (IFM-GEOMAR), Düsternbrooker Weg 20, D-24105 Kiel, Germany.

M.-L. Doan, Laboratoire de Géophysique et Tectonophysique, Université Grenoble 1 (Joseph Fourier), BP 53, F-38041 Grenoble CEDEX 9, France.

N. Efimenko, Institut de Géologie et de Paléontologie, Université de Lausanne, CH-1015 Lausanne-Dorigny, Switzerland.

N. Eguchi, Y. Kido, K. T. Moe, Y. Sanada, K. Takahashi, and S. Toczko, Center for Deep Earth Exploration, JAMSTEC, Showa-machi 3173-25, Kanazawa-ku, Yokohama 236-0001, Japan.

P. Flemings and N. W. Hayman, Institute for Geophysics, Jackson School of Geosciences, University of Texas at Austin, J. J. Pickle Research Campus, Bldg. 196, 10100 Burnet Rd., Austin, TX 78758, USA.

K. Horiguchi, Department of Earth and Space Sciences, Osaka University, 1-1 Machikaneyama, Toyonaka, Osaka 560-0043, Japan.

G. J. Huftile, Biogeosciences Discipline, Queensland University of Technology, GPO Box 2434, Brisbane, Qld 4001, Australia.

T. Ito, Institute of Fluid Science, Tohoku University, 2-1-1 Katahira, Aoba-ku, Sendai 980-8577, Japan.

S. Jiang, Geological Sciences, Florida State University, 108 Carraway Bldg., Tallahassee, FL 32306, USA.

K. Kameo, Department of Earth Sciences, Chiba University, 1-33 Yayoi, Inage, Chiba 263-8522, Japan.

Y. Kano, Research Center for Earthquake Prediction, Disaster Prevention Research Institute, Kyoto University, Gokasho, Uji, Kyoto 611-0011, Japan.

K. Kawabata, Institute of Geophysics, National Central University, 300 Chung-Da Road, Chung Li City, Taoyuan 32001, Taiwan.

A. Kopf, Marum Research Centre, University of Bremen, Leobener Strasse, MARUM Building, D-28359 Bremen, Germany.

W. Lin, Kochi Institute for Core Sample Research,, JAMSTEC, Monobe-otsu 200, Nankoku, Kochi 783-8502, Japan. (lin@jamstec.go.jp)

L. McNeill, National Oceanography Centre, Southampton, University of Southampton, European Way, Southampton SO14 3ZH, UK.

J. C. Moore, Earth and Planetary Sciences Department, University of California, Santa Cruz, CA 95064, USA.

D. Saffer, Geosciences, Pennsylvania State University, 310 Deike Bldg., University Park, PA 16802, USA.

A. M. Schleicher, Department of Geological Sciences, University of Michigan, 2534 CC Little Bldg., 1100 North University Ave., Ann Arbor, MI 48109, USA.

H. Tobin, Department of Geoscience, University of Wisconsin-Madison, 1215 W. Dayton St., Madison, WI 53706, USA.

T. Wiersberg, Section 4.2, GFZ German Research Center for Geosciences, Telegrafenberg, D-14479 Potsdam, Germany.